Available online at www.sciencedirect.com
ScienceDirect
Journal of Power Sources 164 (2007) 134–140
JOURNAL OF POWER SOURCES
www.elsevier.com/locate/jpowsour

# An approach to measuring spatially resolved water crossover coefficient in a polymer electrolyte fuel cell

G.Q. Lu [a], F.Q. Liu [b], Chao-Yang Wang [a,b,*]

[a] *Electrochemical Engine Center (ECEC), Department of Mechanical and Nuclear Engineering, The Pennsylvania State University, University Park, PA 16802, USA*
[b] *Electrochemical Engine Center (ECEC), Department of Materials Science and Engineering, The Pennsylvania State University, University Park, PA 16802, USA*

Received 15 September 2006; received in revised form 9 October 2006; accepted 10 October 2006
Available online 13 November 2006

**Abstract**

This paper reports on an experimental approach to measuring the water crossover coefficient distribution for the first time. A straight-channel PEFC of 6 $cm^2$ segmented into 10 pieces along the reactant flow direction has been developed. The instrumented cell, combining the functions of current collection and gas sampling with one pin for each segment, is capable of measuring current and species distributions simultaneously from a single experiment. The two distribution data are subsequently combined in a material balance analysis to yield the net water transport coefficient distribution through the membrane. For fully humidified anode and partially humidified cathode, the net water transport coefficient is found to range from 0.47 to 0.025, and the electro-osmotic drag dominates water transport through the membrane. For partially humidified anode and cathode, the net water transport coefficient lies between 0.19 and −0.24, with the negative value indicating dominant back diffusion.


*Keywords:* Current distribution; Water distribution; Net water transport coefficient; Water management; Fuel cell diagnostics

## 1. Introduction

Water management is a critical issue impacting performance and durability of polymer electrolyte fuel cells (PEFCs). A quantitative measure of water management is the net water transport coefficient across the membrane, defined as the ratio of the net water flux from the anode to cathode to the protonic flux through the membrane. Physically, the net transport coefficient is a combined result of electro-osmotic drag (EOD), molecular diffusion and hydraulic permeation [1]. The pure EOD coefficient of Nafion membranes is generally believed to be 1.0 over a range of water content up to 14 corresponding to a vapor-equilibrated membrane, and increases to 2.5 in a membrane equilibrated with liquid water or when the water content reaches 22 [2,3].

Prior efforts in the literature to quantify the net water crossover coefficient have been limited to measuring average values through water collection at the anode and cathode exhausts and to performing overall balance [4]. On the other hand, the need for a fundamental understanding of PEFCs has motivated various measurements of distribution data in recent years, such as current and species distributions [5–13]. See Wang [1] for a recent review of various diagnostic methods to obtain current, species and high-frequency resistance (HFR) distributions. Unfortunately, no technique is yet available to measure the distribution of the net water transport coefficient through the membrane.

In this paper, we present a new method to measure the water crossover coefficient distribution using a segmented PEFC developed by Wang group at ECEC that is capable of simultaneously measuring the current distribution, as well as anode water and cathode water distributions [9,12,13]. Further, we choose a straight-channel PEFC of 10 cm length for this study in order to provide benchmark-quality experimental data of current, species and water crossover coefficient distributions for achieving a basic understanding of water management as well as for validating PEFC models.

* Corresponding author. Tel.: +1 814 863 4762; fax: +1 814 863 4848.
*E-mail address:* cxw31@psu.edu (C.-Y. Wang).

0378-7753/$ – see front matter © 2006 Elsevier B.V. All rights reserved.
doi:10.1016/j.jpowsour.2006.10.035

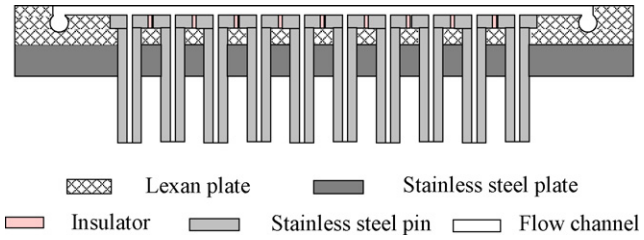


Fig. 1. Schematic of the segmented flow plate.

## 2. Experimental

### 2.1. Cell design

Fig. 1 depicts the design of the segmented cell featuring three straight, parallel channels of 10 cm length. A polycarbonate plate (Lexan) was used for insulation and to embed 10 stainless steel segments. These segments with pins on the back side acted as a flowfield plate to collect current, with a through hole drilled at the center of each segment for gas sampling from the flow channel for species determination. The thick-walled pins collected local current from each segment, and the hole inside each pin was connected to a micro gas chromatograph for species identification. To reduce contact resistance and prevent corrosion, a 30 nm layer of gold was coated on each segment. A plastic insulator was used to separate adjacent segments. A stainless steel plate served as a substrate, and an electrical heater was attached to its surface for temperature control. A T-type thermocouple and a temperature controller were used to maintain the cell temperature at the prescribed value. This unique design of the segmented cell with simplified construction enabled measurement of current distribution and species distributions on both anode and cathode sides, simultaneously. Moreover, the contact resistance between each segment and the gas diffusion layer (GDL) was made sufficiently small and uniform that the experimental data obtained truly reflect the internal characteristics of a non-segmented cell rather than the artificial contact resistance distribution existing in a poorly designed segmented cell.

Fig. 2 shows the flow channels machined into the surface of each segment and neighboring insulators. The flow channels are parallel with three paths. Table 1 summarizes the dimensions of the instrumented cell, with the active area of 6 $cm^2$, and 10 cm × 0.6 cm segments. While the channel areas are 0.3 $cm^2$ in each segment, the land area that physically contacts the MEA is only 0.264 $cm^2$ owing to the existence of insulators between two conducting segments. The fractional locations of the segment centers are $x/L = 0.05$, 0.15, 0.25, 0.35, 0.45, 0.55, 0.65, 0.75, 0.85, and 0.95 from the cathode inlet.

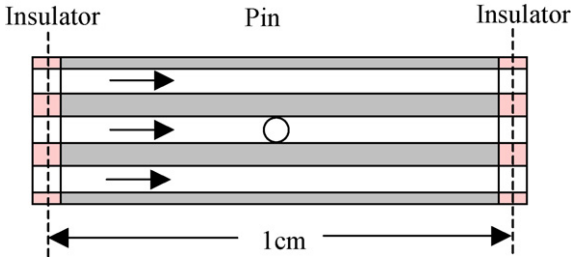


Fig. 2. Schematic of flow channels in each segment.

Table 1
Dimensions of the instrumented cell

| | |
|---|---|
| Length of the pin (mm) | 8.8 |
| Width of the pin (mm) | 6 |
| Number of flow channels | 3 |
| Width of the flow channel (mm) | 1 |
| Depth of the flow channel (mm) | 0.5 |
| Diameter of sampling hole (mm) | 1 |
| Length of plastic insulator (mm) | 1.2 |
| Effective area of each segment ($cm^2$) | 0.6 |
| Number of segments | 10 |
| Total effective area of MEA ($cm^2$) | 6 |

Gore-Select membrane (EW = 950) of 30 μm thickness was used in the experiments. Carbon paper coated with microporous layer was used as the gas diffusion layer, without segmentation, for both anode and cathode. The baseline operating conditions in the experiments were set at: (1) absolute pressure of 2 atm for both air in the cathode and pure hydrogen in the anode; (2) cell temperature of 80 °C; (3) stoichiometric flow ratio of 2 @ 1 A $cm^{-2}$ for both anode and cathode; and (4) co-flow between the anode and cathode flows.

### 2.2. Measurement apparatus

Fig. 3 displays a schematic of the experimental setup. Ten pairs of pins in the test cell were connected to 10 independent channels of a multi-channel potentiostat (Arbin). By measuring the local currents of 10 segments (or sub-cells) simultaneously, the current distribution in the operating cell was mapped. To measure the species concentrations in both anode and cathode flows, 10 gas sampling stainless steel tubes with outer diameter of 1/16 in. were connected to a multi-inlet and one-outlet microelectric actuator (Valco) on each side of the fuel cell. The microelectric actuator can selectively switch to one of 10 inlet ports for connection with the gas chromatograph column by remote control. The gas sample was then sucked into a micro gas chromatograph (micro GC, Agilent) for species identification. To avoid water condensation, the sampling tubes, the automatic valve body of the microelectric actuator, and the inlet port of the micro GC were all heated above120 °C. In the micro GC, two columns separate the species – a Plot-U column, and a molecular sieve column with a backflush module to prevent excess water damage. The carrier gas used was helium in the Plot-U column for water measurements, and argon in the molecular sieve column for $H_2$, $O_2$, and $N_2$ measurements, respectively. The pressures of both carrier gases were controlled at 80 psi in all experiments to improve accuracy of measurements.

The amount of gas sampled by the micro GC was negligibly small (about 20 μl for each run), thus ensuring uninterrupted operation of the cell. The micro GC was calibrated in advance. More details on GC calibration may be seen in Ref. [13]. Between 40 °C and 85 °C, the maximum relative error was found to be less than 4.5%. Species concentration was usually measured three or more times and an average of the data taken

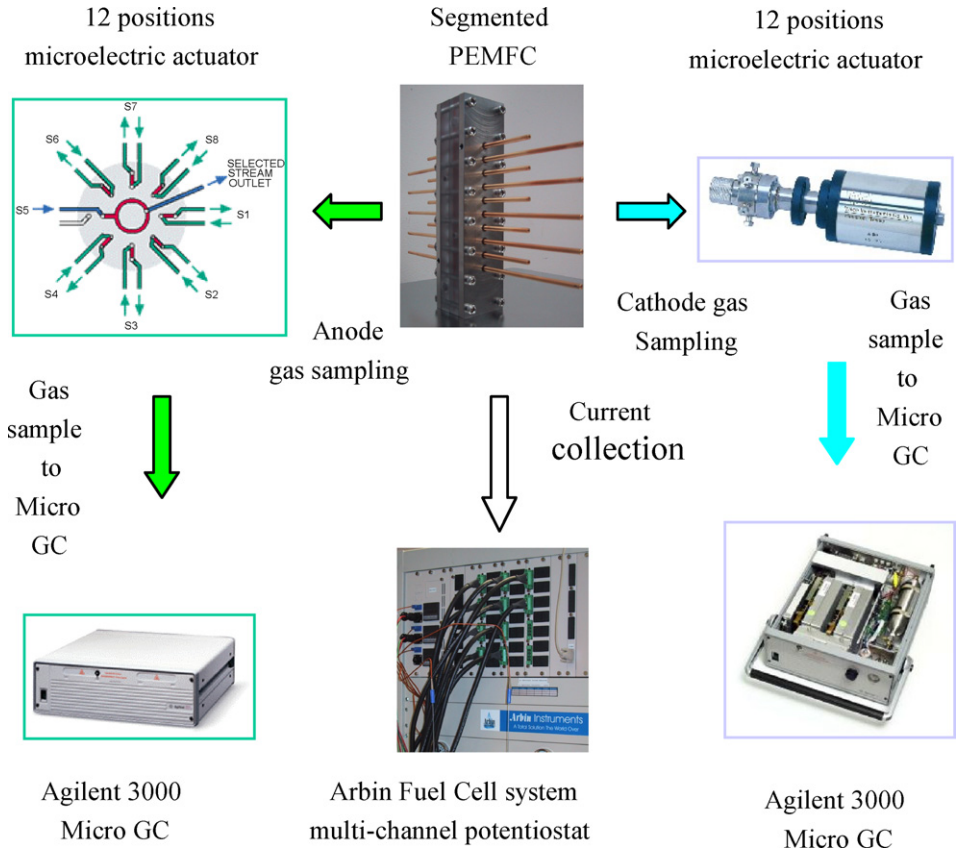


Fig. 3. Experimental setup for measurement of current and species distributions in a segmented PEFC.

for each condition to minimize the random error. To measure the species distributions in the anode and cathode simultaneously, two sets of microelectric actuators and micro GCs were deployed as shown in Fig. 3.

## 3. Material balance analysis

To deduce the net water transport coefficient through the membrane, we consider a differential volume around pin $j$ (where $j = 1$–$10$) with two halves of the neighboring plastic insulators, as shown in Fig. 4. Under steady-state operation, a material balance analysis over the differential volume on the anode side dictates that the net water transport from the anode to cathode is equal to the water loss for the flow through the control volume in the anode, i.e.,

$$\alpha \frac{I_j A_j}{F} = \dot{m}^{\mathrm{H_2O}}_{\mathrm{a},j-1} - \dot{m}^{\mathrm{H_2O}}_{\mathrm{a},j} \tag{1}$$

where $\alpha$ is the net water transport coefficient, $A_j$ the active area of the control volume, $F$ the Faraday constant, $I_j$ the local current density of segment $j$, and $\dot{m}$ is the molar flow rate. Here the subscript 'a' denotes the anode side.

The water molar flow rate in Eq. (1) can be determined from:

$$\dot{m}^{\mathrm{H_2O}}_{\mathrm{a},j} = \frac{X^{\mathrm{H_2O}}_{\mathrm{a},j}}{1 - X^{\mathrm{H_2O}}_{\mathrm{a},j}} \dot{m}^{\mathrm{H_2}}_{\mathrm{a},j} \tag{2}$$

where $X$ is the mole fraction. The hydrogen molar flow rate is calculated by

$$\dot{m}^{\mathrm{H_2}}_{\mathrm{a},j} = \dot{m}^{\mathrm{H_2}}_{\mathrm{a},j-1} - \frac{I_j A_j}{2F} \tag{3}$$

At the anode inlet, the hydrogen molar flow rate is given according to the stoichiometry and relative humidity. That is,

$$\dot{m}^{\mathrm{H_2}}_{\mathrm{a},0} = \xi_{\mathrm{a}} \frac{I_{\mathrm{ref}} \sum A_j}{2F} \tag{4}$$

where $\xi$ is the stoichiometry at the reference current density $I_{\mathrm{ref}}$. The water molar flow rate at the inlet can be calculated by Eq.

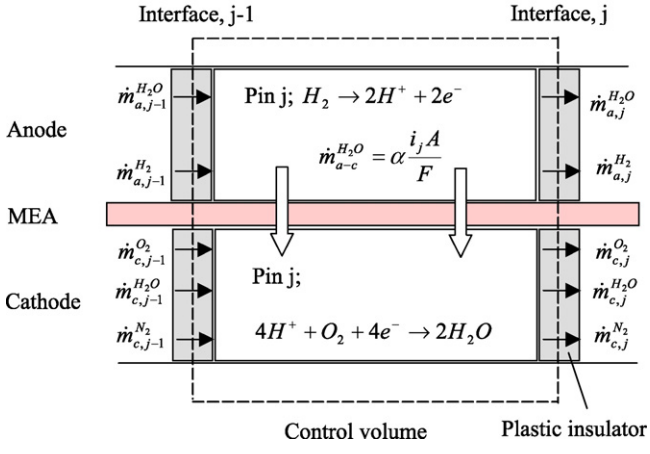


Fig. 4. Control volume for material balance analysis.

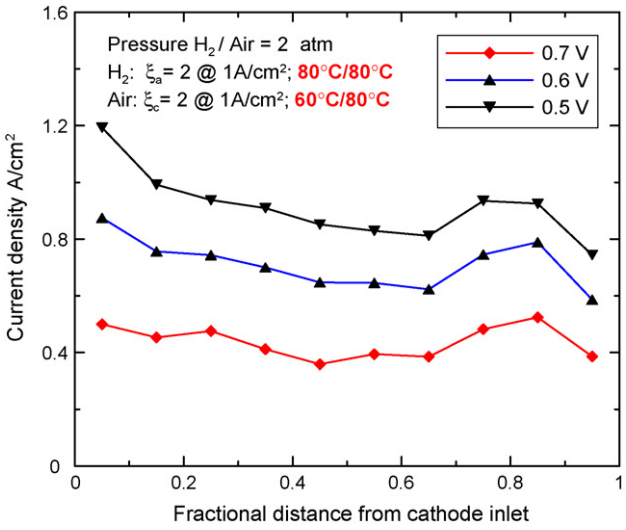


Fig. 5. Current distributions at various voltages for the humidifier temperature of 60 °C in the cathode and 80 °C in the anode. The cell temperature is 80 °C.

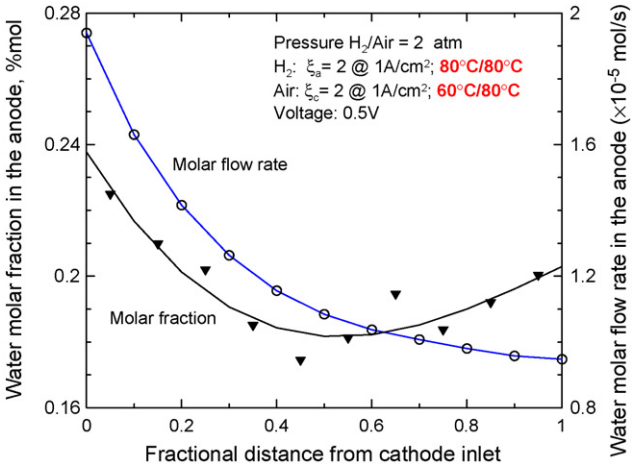


Fig. 6. Water molar concentration and molar flow rate in the anode for the humidifier temperature of 60 °C in the cathode and 80 °C in the anode. The cell temperature is 80 °C. For the water molar fraction, solid symbols stand for experimental data and the line is a fitted curve. The molar flow rate curve is calculated from the fitted molar fraction curve.

(2), where the water mole fraction at the inlet is determined by the humidifier temperature.

By measuring the local current density and mole fraction of water in the anode, the net water transport coefficient distribution, $\alpha(x)$, can be then calculated according to Eq. (1). Additionally, profiles of the gas volumetric flow rate and density along the anode channel can be determined from Eqs. (1)–(4). The latter information may be useful for calculating the anode pressure drop accurately and verifying the constant gas density approximation in the anode, a commonly invoked assumption in PEFC models.

Similarly, a differential volume analysis can be performed on the cathode side, as illustrated in Fig. 4. Here, the difference in the water molar flow rate between two faces of the control volume is attributed to the net water transport from the anode side as well as to that produced from oxygen reduction reaction (ORR). If using the net water transport coefficient determined from the control volume analysis in the anode as well as the measured local current density, one can use the cathode control volume analysis to compute the water and oxygen mole fraction distributions in the cathode. Such calculated results will then be compared to the actually measured experimental data for further validation of the present approach.

## 4. Results and discussion

### 4.1. Low inlet humidity in the cathode

Fig. 5 shows the current distribution at different cell voltages with humidification temperature of 53 °C in the cathode and 80 °C in the anode. The cell temperature was maintained at 80 °C. Thus, the cathode features low inlet relative humidity of $RH_c = 30\%$. The average current densities reach 0.44 A cm$^{-2}$, 0.71 A cm$^{-2}$, and 0.91 A cm$^{-2}$ at 0.7 V, 0.6 V, and 0.5 V, respectively. These high average current densities are indicative of negligibly small contact resistances involved in the present test cell. At a higher voltage (0.7 V), the average current density is smaller. Therefore, the real stoichiometry along the flow path is relatively large. Consequently, the current density distribution is relatively uniform at higher voltages. At lower voltages, the current density is higher at the cathode inlet and decreases along the flow, due to $O_2$ depletion effect. Along the flow path, there is a local increase in the current density near $x/L = 0.75$, as shown in Fig. 5. This is likely due to the water concentration on the anode side increasing again after experiencing a minimum point (see Fig. 6), thus lowering the membrane resistance. The current density at the fractional location $x/L = 0.95$ is relatively low, perhaps due to the existence of a large local contact resistance in the last sub-cell. The flooding effect may not play a role in these experiments, as the relative humidity near the exit is still a little lower than the saturation concentration as to be seen from the water distribution data shortly. Furthermore, later in this paper we shall show that the current density at $x/L = 0.95$ remains low even with use of low inlet humidity gases in both the anode and cathode when the outlet humidity is far below the saturation level.

Fig. 6 depicts the water mole fraction and water molar flow rate distributions in the anode along the flow channel at the cell voltage of 0.5 V. The solid symbols shown in Fig. 6 represent the experimental measurements of water mole fraction, and the line is a best fit to facilitate mathematical manipulation to extract the net water transport coefficient as detailed in the preceding section. The molar flow rate shown in Fig. 6 is calculated from the material balance analysis presented earlier. As can be seen from Fig. 6, the water mole fraction and molar flow rate both decrease along the flow in the inlet region, due to the electro-osmotic drag and perhaps also forward water diffusion from the anode to cathode.

Between the middle portion and the exit region of the anode channel, the water molar flow rate continues to decrease, whereas the water mole fraction is seen to increase along the flow (see Fig. 6). Theoretically, this reverse profile occurs when the hydrogen consumption rate overrides that of water loss from the

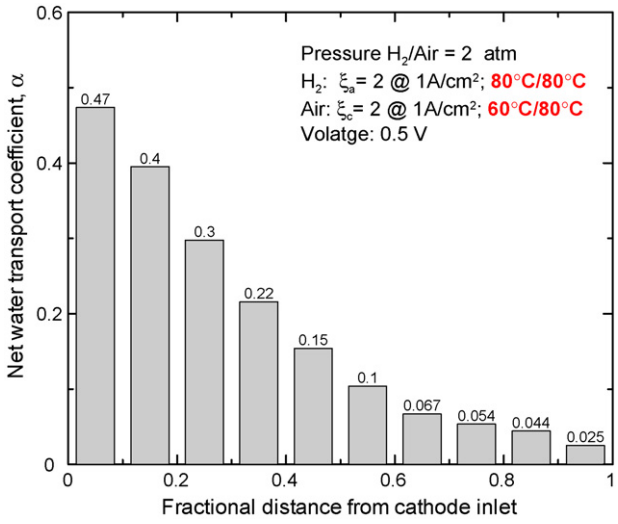


Fig. 7. Net water transport coefficient profile for the humidifier temperature of 60 °C in the cathode and 80 °C in the anode. The cell temperature is 80 °C.

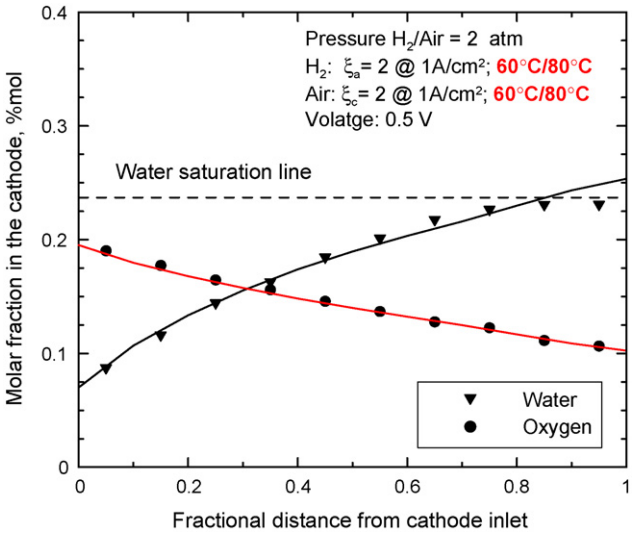


Fig. 8. Water and oxygen molar concentration distributions in the cathode for the humidifier temperature of 60 °C in the cathode and 80 °C in the anode. The cell temperature is 80 °C. The solid symbols are experimental data and the lines are calculated results based on the determined net water transport coefficient.

anode to cathode. Fig. 6 provides the first experimental evidence of this physical phenomenon.

Based on the material balance analysis presented earlier and the measured current distribution in the cell and water distribution in the anode presented in Figs. 5 and 6, we can determine the net water transport coefficient distribution. Fig. 7 shows the resulting water crossover coefficient as a function of the flow fractional distance at the cell voltage of 0.5 V. The net water transport coefficient through the membrane is highest near the inlet region and decreases along the flow channel from 0.47 to 0.025. As said before, the net water transport coefficient is the combined effect of the electro-osmotic drag and water diffusion. The EOD coefficient in fluorinated membranes, such as the one used in this study, is expected to be unity in the water content range considered. The maximum $\alpha$ of only 0.47 implies back diffusion of water from the cathode to anode despite that the anode gas channel has much higher water concentration than the cathode gas channel. Our hypothesis here is that upon current load, the local water concentration in the cathode catalyst layer, which is the driving force for water diffusion through the membrane, is actually higher than that on the anode side, as well as in the cathode gas channel. In other words, the cathode catalyst layer acts as a watershed to diffuse water towards the cathode gas channel as well as the anode side. This explains why the net water transport coefficient decreases along the flow channels.

Janssen and Overvelde [4] reported the net water transport coefficient between 0 and 0.2 using saturated hydrogen in the anode at 80 °C. Recently, Yang et al. [13] also presented a similar result. From the distribution of the net water transport coefficient shown in Fig. 7, the mean net water transport coefficient can be calculated to be about 0.18. Our results show a similar tendency with those of Janssen and Overvelde [4] and Yang et al. [13].

Fig. 8 elaborates a comparison between experimental data and calculated results of water molar fraction and oxygen molar fraction in the cathode. The good agreement for both the oxygen and water shown in Fig. 8 indicate that the net water transport coefficients shown in Fig. 6 are calculated accurately. Shown in Fig. 8, the oxygen molar fraction steadily decreases because of the consumption by electrochemical reaction. The water molar concentration increases along the flow channel due to water production. A comparison of water molar concentrations in the anode shown in Fig. 5 and in the cathode shown in Fig. 8 indicates that water diffusion is from anode to cathode near the inlet and reverses its direction near the outlet. This fact further explains why the net water transport coefficient decreases along the channel as shown in Fig. 7.

### 4.2. Low humidity in both anode and cathode

Fig. 9 displays current distribution at various voltages with dew point temperatures of 53 °C and 56 °C in the anode and

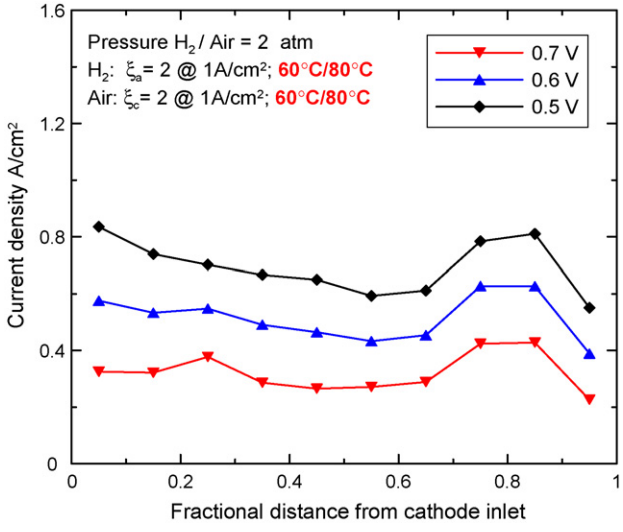


Fig. 9. Current density profiles at various voltages for the humidifier temperature of 60 °C in both anode and cathode. The cell temperature is 80 °C.

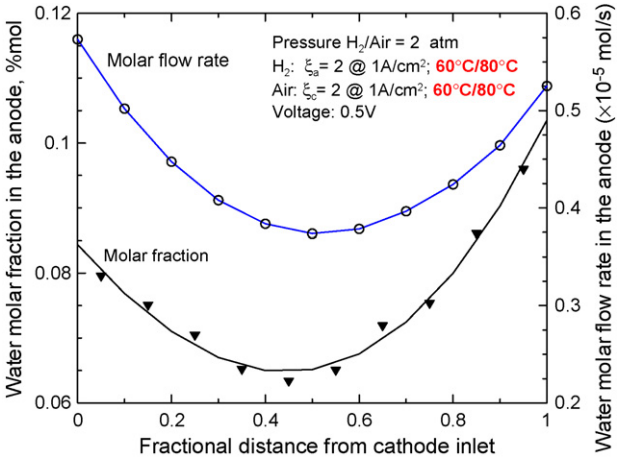


Fig. 10. Water molar concentration and molar flow rate in the anode for the humidifier temperature of 60 °C in both anode and cathode. The cell temperature is 80 °C. For the water molar fraction, solid symbols stand for experimental data and the line is a fitted curve. The molar flow rate curve is calculated from the fitted molar fraction curve.

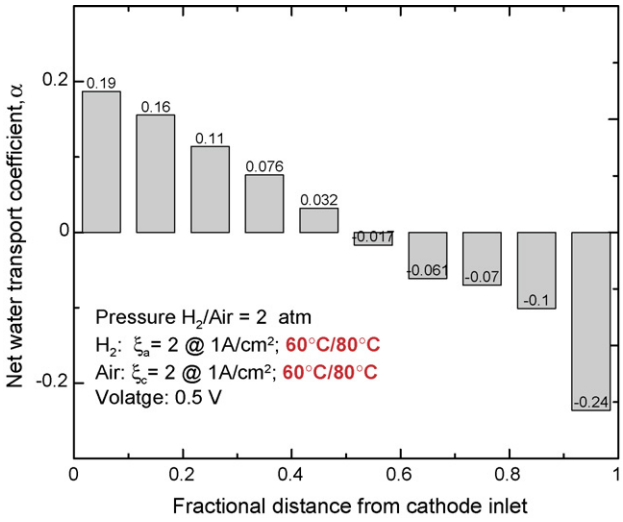


Fig. 11. Net water transport coefficient profile for the humidifier temperature of 60 °C in both anode and cathode. The cell temperature is 80 °C.

cathode inlet gases, respectively. The cell temperature is still maintained at 80 °C. Current distribution at different voltages is relatively uniform and the overall performance is low. At 0.5 V, the mean current density is only about 0.61 A $cm^{-2}$. The membrane is relatively dehydrated under low humidity, resulting in low cell performance. At $x/L = 0.95$, the current density is unreasonably low, possibly caused by unexpected large contact resistance there.

The corresponding distributions of the water molar fraction and molar flow rate in the anode at 0.5 V are illustrated in Fig. 10. Similarly, the fitted curve of the water molar fraction is based on the experimental data, and the water molar flow rate is derived from the material balance. Shown in Fig. 10, both the molar fraction and the molar flow rate tend to increase again near the channel exit. This fact implies that the net water flux directs from the cathode to anode near the channel exit. In other words, the water back diffusion is the dominating effect compared to the electro-osmotic effect in this region. The trend of the molar flow rate is different from that for the saturated anode inlet shown in Fig. 6 where the electro-osmotic drag dominates over back diffusion.

Fig. 11 displays the derived net water transport coefficient distributions along the flow path. Near the inlet, the water transport coefficient is positive, signifying that net water transport is from anode to cathode. Notice that the maximum net water transport coefficient is only 0.19 at the first segment, despite that water concentrations in the anode and cathode gas channels are very close. However, the water concentration at the cathode/membrane interface must be higher due to water production from oxygen reduction reaction, thus driving water back diffusion from the cathode to anode to offset the EOD through the membrane. Fig. 11 also shows that the net water transport coefficient decreases along the flow channel due to enhanced back diffusion. With the difference in water concentrations across the membrane increased, the water back diffusion eventually dominates over the EOD; consequently, the net water transport coefficient becomes negative. The lowest net water transport coefficient shown in Fig. 11 is −0.24, consistent with the results of Janssen and Overvelde [4].

Fig. 12 shows the axial profiles of oxygen and water molar concentrations in the cathode. Again, the experimental data show good agreement with the calculated results based on the net water transport coefficients shown in Fig. 11. The oxygen molar concentration displays a monotonous decrease along the flow channel, as expected. The water molar concentration steadily increases along the flow. Compared to the water molar concentration in the anode shown in Fig. 10, the water concentration in the cathode channels is higher than that in the anode, resulting in water diffusion from the cathode to anode under these operating conditions.

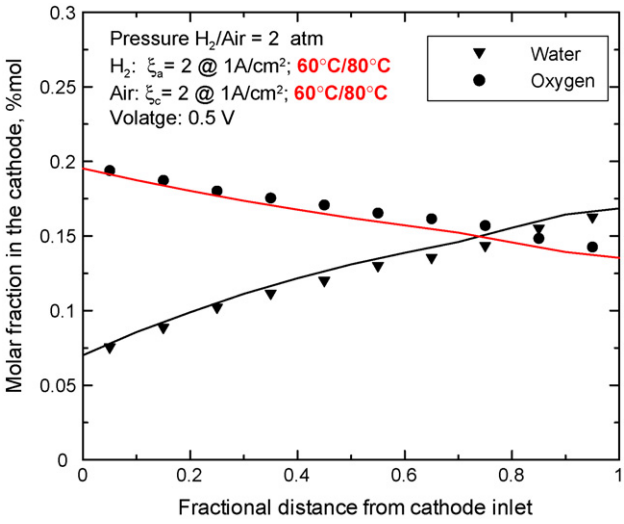


Fig. 12. Water and oxygen molar concentration profiles in the cathode for the humidifier temperature of 60 °C in both anode and cathode. The cell temperature is 80 °C. The solid symbols stand for experimental data and the lines are calculated results based on the determined net water transport coefficient.

## 5. Conclusion

We have reported a novel method to determine the net water transport coefficient distribution by simultaneously measuring current and water distributions in a segmented PEFC. The experimental data of the net water transport coefficient distribution along flow channels in a co-flow $H_2$/air cell were presented for the first time in the literature. Water transport through the membrane as controlled by EOD and back diffusion has been studied in a range of anode and cathode inlet RH. The water concentration in the anode gas channel is found to decrease along the flow near the anode inlet due to the dominant EOD effect, but to increase again towards the channel exit once the cathode water concentration is built up from ORR. With a fully humidified anode and a partially humidified cathode, the net water transport coefficient through the membrane decreases from 0.47 to 0.025 along the flow. Under partial humidification of both anode and cathode, the net water transport coefficient is between 0.19 and −0.24, with the negative value indicating strong back diffusion of water through the membrane. The water and oxygen profiles in the cathode computed based on the determined net water transport coefficient show a good agreement with the actual experimental data, demonstrating good water balance between the anode and cathode water measurements. The data of $\alpha$-distribution presented in this paper and a companion paper [14] are useful for the validation of computational fuel cell models.

## Acknowledgements

Financial support of this work from ECEC industrial sponsors is gratefully acknowledged. The authors are also thankful for useful discussions with Dr. X.G. Yang and Mr. Nick Burke as well as valuable input received from 2005 Gordon Research Conference on Fuel Cells where this work was first presented.

## References

[1] C.Y. Wang, Chem. Rev. 104 (2004) 4727.
[2] T.F. Fuller, J. Newman, J. Electrochem. Soc. 139 (1992) 1332.
[3] T.A. Zawodzinski Jr., J. Davey, J. Valerio, S. Gottesfeld, Electrochim. Acta 40 (1995) 297.
[4] G.J.M. Janssen, M.L.J. Overvelde, J. Power Sources 101 (2001) 117.
[5] J. Stumper, S.A. Campbell, D.P. Wilkinson, M.C. Johnson, M. Davis, Electrochim. Acta 43 (1998) 3773.
[6] S.J.C. Cleghorn, C.R. Derouin, M.S. Wilson, S. Gottesfeld, J. Appl. Electrochem. 28 (1998) 663.
[7] C. Wieser, A. Helmbold, E. Gulzow, J. Appl. Electrochem. 30 (2000) 803.
[8] D.J.L. Brett, S. Atkins, N.P. Brandon, V. Vesovic, N. Vasileiadis, A.R. Kucernak, Electrochem. Commun. 3 (2001) 628.
[9] M.M. Mench, C.Y. Wang, M. Ishikawa, J. Electrochem. Soc. 150 (2003) A1052.
[10] M. Noponen, J. Ihonen, A. Lundblad, G. Lindbergh, J. Appl. Electrochem. 34 (2004) 255.
[11] A. Hakenjos, H. Muenter, U. Wittstadt, C. Hebling, J. Power Sources 131 (2004) 213.
[12] M.M. Mench, Q.L. Dong, C.Y. Wang, J. Power Sources 124 (2003) 90.
[13] X.G. Yang, N. Burke, C.Y. Wang, K. Tajiri, K. Shinohara, J. Electrochem. Soc. 152 (2005) A759.
[14] F. Liu, G. Lu, C.Y. Wang, Water transport coefficient distribution through the membrane in a polymer electrolyte fuel cell, J. Membr. Sci. 287 (2007) 126–131.